A Smart Model for Welding Engineers to Achieve Target Fusion Zone Geometry and Microstructure using Parallel Genetic Algorithm

A. Kumar
Department of Materials Science and Engineering
The Pennsylvania State University,
PA 16802, USA

S. Mishra
Department of Materials Science and Engineering
The Pennsylvania State University,
PA 16802, USA

Abstract

A smart, bi-directional model has been developed to determine three-dimensional temperature profiles, weld geometry and the transformed phase fraction during gas tungsten arc (GTA) butt welding. The model is capable of estimating input parameters such as the net input power, welding speed, effective thermal conductivity, and, activation energy, pre-exponential factor and exponent in Johnson-Mehl-Avrami (JMA) equation for phase transfer calculations, using limited number of experimental data and parallelized Parent Centric Recombination (PCX) based Generalized Generation Gap (G3) genetic algorithm as a multivariable optimization technique. Thus, the model can satisfy both the industrial and research requirements of specifying a window of input parameters to obtain specific weld geometry and calculating uncertain input parameters required during mathematical modeling. The calculated shape and size of the fusion zone and the austenite phase fraction were in fair agreement with the experimental results. The effect of various parameters on convergence and reliability of the proposed multiple deme based G3 model was also studied. The model gave increased reliability and faster convergence.

1 INTRODUCTION

Reliable and cost-effective welds are often fabricated in industry through repeated experiments and experience. However, this approach ignores the potential technological advantage attainable through the application of principles of modern welding science and technology. Efforts to correlate large number of welding variables with weld characteristics through neural network or statistical regression are expensive and time consuming because of the requirement of a large number of welding experiments (De and DebRoy, 2004). In the last decade, phenomenological models of fusion welding have provided important understanding of the welding processes and welding materials (David and DebRoy, 1992). However, these models can only predict weld characteristics for a given set of input welding variables, whereas the welding engineers need a window of operating variables to produce a weld with target weld characteristics such as weld geometry. The mismatch between the industrial needs and the structure of the currently available phenomenological models has restricted the use of these powerful computational models in the industry. The approach outlined in this paper empowers practicing engineers to determine a window of input variables that would provide the target weld geometry and microstructure. This work will add to the growing quantitative knowledge base in welding industry aided by the promise to solve difficult problems using concepts of evolution and increasing powers of modern software and hardware.

Current computer models for the calculation of heat transfer and phase transformations in gas tungsten arc (GTA) butt welding require many input parameters to define the welding system, such as the system geometry, welding variables, Johnson-Mehl-Avrami (JMA) kinetic parameters (Elmer et al., 2003) and thermo-physical data. Several of these parameters such as the thermo-physical properties, system geometry, welding current (I), voltage (V) and welding speed can be easily specified with a reasonable degree of certainty. However, for GTA welding process, values of net power input to the workpiece ($I \times V \times$ arc efficiency), effective thermal conductivity, and activation energy of phase transformation, pre-exponential factor and exponent in JMA equation cannot be assigned easily. Although the values of arc efficiency, which determines the net power input to the workpiece, have been experimentally measured for many welding conditions, the reported values vary significantly even for apparently similar welding conditions, reflecting the complexity of the welding processes (Kumar et al., 2004). The value of

effective thermal conductivity is the property of the specific welding system and not an inherent thermo-physical property of the liquid metal, and hence needs to be estimated (De and DebRoy, 2004). (Nath et al., 1994) have shown that due to the effect of nucleation and growth on phase transformation kinetics, the apparent activation energy for diffusion of carbon in austenite will be different from the actual value. As the JMA equation is modified to capture the non-isothermal behavior of the system, the JMA pre-exponential factor and exponent need to be calculated accurately. (Elmer et al., 2003) calculated the values of pre-exponential and exponent parameters of JMA equation by taking the value of activation energy suggested by (Nath et al., 1994) and using curve fitting technique. However, as the values of these kinetic parameters are very sensitive to the value of activation energy, therefore, activation energy also needs to be considered as an unknown variable in the calculations. Currently there is no unified basis to accurately prescribe the values of these variables based on scientific principles. Since the results obtained from the heat transfer and phase transformation models depend significantly on these input parameters, it is necessary to determine them accurately.

A recourse is to develop an inverse modeling scheme utilizing the power of phenomenological heat transfer and JMA based phase transformation models to calculate the optimum values of these unknown variables using a limited amount of experimental data. (De and DebRoy, 2003; Kumar et al., 2004; and Kumar and DebRoy, 2004) calculated the unknown values of a few input parameters like arc efficiency and effective thermal conductivity using the weld pool dimensions as experimental data. In their models, they used numerical derivative based optimization techniques to find the values of input parameters. The output from these models is a single set of values of the input parameters. However, in GTA welding process, the evolution of weld pool involves complex interaction of physical processes such as application of welding arc, heat transfer and phase transformation. To simulate these simultaneous processes for obtaining the target weld geometry and microstructure, several combinations of welding variables are possible. The ability of genetic algorithm (GA) to find multiple optimal solutions and provide a window of parameters makes it unique in solving inverse problems having multiple solutions (Back et al., 2000).

Two interactive computational modules will be embedded into the proposed GTA butt weld smart model for welding engineers – one for the analysis of heat transfer using Rosenthal solution in fusion butt welding (Sista et al., 2000) and calculation of phase transformation using JMA equation (Elmer et al., 2003), and the other for the optimization of the unknown parameters using Parent Centric Recombination (PCX) based Generalized Generation Gap (G3) genetic algorithm model (Deb et al., 2002; Deb, 2003). The approach adopted here will be inherently different from the neural network technique where the input and output variables are related through a set of hidden nodes and their relationships do not have to comply with any physical law. In contrast, when the optimization algorithm embodies a phenomenological model of heat transfer and modified JMA equation to take into account non-uniform weld heating and transformation in $\alpha+\gamma$ two-phase field (α or ferrite is the low temperature phase, and γ or austenite is the high temperature phase of steel), the window of welding parameters and the output weld pool geometry and microstructure are related by phenomenological governing laws. Thus, the present smart model, equipped with the phenomenological models based on physical laws will be able to provide a quantitative framework for practicing engineers to achieve the target weld geometry and microstructure.

The goal of the present work is to estimate the net input power, effective thermal conductivity, welding speed, activation energy of transformation, and pre-exponential factor and exponent of JMA equation through an inverse modeling approach, which includes a combination of a genetic algorithm based optimization model, a temperature field calculation model, a phase fraction calculation model and a set of experimentally measured data. To reduce the computation time, a parallel version of PCX based G3 model based on island model approach (Back et al., 2000) is developed and the effect of various migration parameters on convergence is analyzed.

2 EXPERIMENTAL DATA

Tables 1 and 2 present the experimentally measured values of austenite phase fractions and temperatures used in the present study (Elmer et al., 2003).

Table 1: Experimental data for austenite (γ) phase fractions along x = -3.5 mm line on the top surface (z = 0)

LOCATION (mm)	γ-PHASE FRACTION
(-3.5, 3.25, 0)	1.000
(-3.5, 3.50, 0)	0.989
(-3.5, 3.75, 0)	0.939
(-3.5, 4.00, 0)	0.778
(-3.5, 4.25, 0)	0.480
(-3.5, 4.50, 0)	0.287
(-3.5, 4.75, 0)	0.103
(-3.5, 5.00, 0)	0.040
(-3.5, 5.25, 0)	0.014
(-3.5, 5.50, 0)	0.000

Table 2: Experimental data for temperature at different locations on the top surface ($z = 0$)

LOCATION (mm)	TEMPERATURE (K)
(5.0, 0, 0)	1727.978
(8.0, 0, 0)	1191.736
(10.5, 0, 0)	978.942
(-3.5, 0, 0)	1770.002
(-5.0, 0, 0)	1193.387
(0, 4.0, 0)	1780.218

3 MATHEMATICAL MODEL

The proposed work is based on coupling an optimization model with phenomenological models of heat transfer and phase fraction calculations and a limited volume of experimental data to achieve a useful smart model for welding engineers. The optimization algorithm minimizes the objective function (i.e. squared error between the predicted and the experimentally observed temperatures and austenite phase fractions) during the GTA welding process.

3.1 DIRECT NUMERICAL MODEL

3.1.1 Calculation of temperature field

The temperature field is calculated using Rosenthal's analytical equation (Sista et al., 2000; Lambrakos and Milewski, 2002; Karkhin et al., 2002):

$$T = T_o + \frac{P}{2\pi kr}\exp\left(-\frac{v(r-x)}{(2k/\rho C)}\right) \quad (1)$$

where T_o is the ambient temperature (K), P is the net power input (W), k is the effective thermal conductivity ($W/m\text{-}K$), r is the distance of a given location from the heat source (m), v is the welding velocity (m/s), x is the x-coordinate of the given location (m), ρ is the density of the material (kg/m^3), and C is the specific heat of the material ($J/kg\text{-}K$). From the calculated temperature field, the thermal cycles, i.e. the temperature versus time data at a given location, are calculated by dividing the x-coordinate by the welding velocity.

3.1.2 Calculation of austenite (γ) phase fraction

The austenite phase fraction, fr, at selected locations is calculated using the non-isothermal JMA equation (Elmer et al., 2003):

$$\frac{fr(t_i)}{F_i} = 1 - \exp\left\{-\left[k_o \times \exp\left(-\frac{Q}{RT_i}\right)\times(\Delta t + \tau_i)\right]^n\right\} \quad (2)$$

$$\text{for } 1 \le i \le m$$

where T_i is the temperature for the i^{th} interval (K), F_i is the equilibrium fraction of the new phase at temperature T_i, k_0 is a pre-exponential constant (s^{-1}), Q is the activation energy for phase transformation (kJ/mol), R is the gas constant, Δt is the time interval (s), m is the number of time steps in the thermal cycle, n is the JMA exponent, and τ_i is a time constant given by:

$$\tau_i = \frac{\sqrt[n]{-\ln\left[1-\frac{fr(t_{i-1})}{F_i}\right]}}{k_0 \times \exp\left(-\frac{Q}{RT_i}\right)} \quad (3)$$

where $fr(t_{i-1})$ is the fraction calculated at the end of $(i\text{-}1)^{th}$ time step. This equation is for the i^{th} time interval, t_i, and has to be integrated over the thermal cycle at a location, obtained from the heat transfer model, to get the austenite phase fraction, fr, at that location.

3.2 GENETIC ALGORITHM AS AN OPTIMIZATION MODEL

The objective function is defined as:

$$\min O = \sum_{i=1}^{n}\sum_{j=1}^{m}\left(\frac{T^c(x_i, y_j, 0)}{T^e(x_i, y_j, 0)} - 1\right)^2 + \sum_{k=1}^{p}\sum_{l=1}^{q}\left(\frac{fr^c(x_k, y_l, 0)}{fr^e(x_k, y_l, 0)} - 1\right)^2 \quad (4)$$

where $T^e(x_i, y_j, 0)$ and $T^c(x_i, y_j, 0)$ are the experimental and calculated absolute temperatures at location $(x_i, y_j, 0)$, respectively, and $fr^e(x_k, y_l, 0)$ and $fr^c(x_k, y_l, 0)$ represent the experimental and calculated values of austenite phase fractions at location $(x_k, y_l, 0)$, respectively. In Eq. (4), objective function, O, is a function of some known parameters (e.g. ρ, C, r, T_o etc.) and six unknown parameters, i.e. net power (P), welding velocity (v), effective thermal conductivity (k), pre-exponential constant (k_0), activation energy for phase transformation (Q) and JMA equation exponent (n).

$$O = f(P, v, k, k_0, Q, n) \quad (5)$$

Therefore, we need to find six unknown parameters to minimize the value of objective function, which depends non-linearly on these variables as shown by Eqs. (1), (2), (3) and (4).

The Generalized Generation Gap (G3) model using Parent Centric Recombination (PCX) operator (Deb et al., 2002; Deb, 2003) is used in the present study for optimizing the values of the unknown variables. This model was chosen because it has been shown to have faster convergence rate on standard test functions as compared to other evolutionary algorithms (Deb et al., 2002; Deb, 2003). This model is a modification of Minimal Generation Gap (MGG) model (Deb et al., 2002). In this model, the roulette-wheel selection of MGG model is replaced by block selection of best two solutions. This is a steady state

model, which preserves elite solution from the previous iteration as shown in Fig. 1.

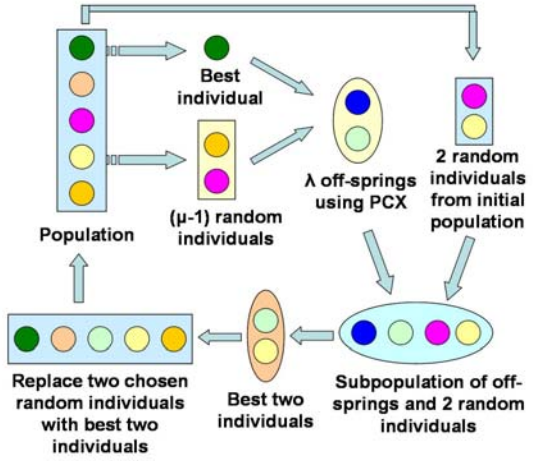

Figure 1: Generalized Generation Gap (G3) model using PCX operator

3.2.1 Algorithm of PCX based G3 model

The algorithm of the G3 model is as follows:

1. From the population, *P(t)*, select the best parent and *μ-1* other parents randomly.
2. Generate λ offspring from the chosen μ parents using a recombination scheme.
3. Choose two parents at random from the population.
4. From a combined subpopulation with two chosen parents and λ created offspring, choose the best two solutions and replace the chosen two parents with these solutions.

The G3 model uses a Parent Centric Recombination (PCX) operator in step 2, which is a modification of Unimodal Normal Distributed Crossover (UNDX) operator. The main difference from UNDX operator is that the offspring solutions are centered around each parent in PCX operator as shown in Fig. 2.

In PCX operator, first, the mean vector $\vec{g}$ of the chosen μ parents is computed. For each offspring, one parent $\vec{x}^{(p)}$ is chosen with equal probability. The direction vector $\vec{d}^{(p)} = \vec{x}^{(p)} - \vec{g}$ is calculated as shown in Fig. 2(c). Thereafter, from each of the other *(μ-1)* parents, perpendicular distances D_i to the line $\vec{d}^{(p)}$ are computed and their average $\bar{D}$ is found (Fig. 2(c)). The offspring is created as follows (Deb et al., 2002):

$$\vec{y} = \vec{x}^{(p)} + w_\zeta \left|\vec{d}^{(p)}\right| + \sum_{i=1, i\neq p}^{\mu} w_\eta \bar{D} \vec{e}^{(i)} \qquad (6)$$

where $\vec{e}^{(i)}$ are the *(μ-1)* orthonormal bases that span the subspace perpendicular to $\vec{d}^{(p)}$. Thus the complexity of the PCX operator is $O(\mu)$, instead of $O(\mu^2)$ required for the UNDX operator. The parameter w_ζ and w_η are zero-mean normally distributed variables with variance σ_ζ^2 and σ_η^2, respectively. In this approach, individual recombination operator biases offspring to be created near the parents by assigning each parent an equal probability of creating offspring in its neighborhood. The selection operation reduces the variance in the population whereas PCX operator increases it. This ensures that population mean of the entire offspring population is identical to that of the parent population (Deb et al., 2002).

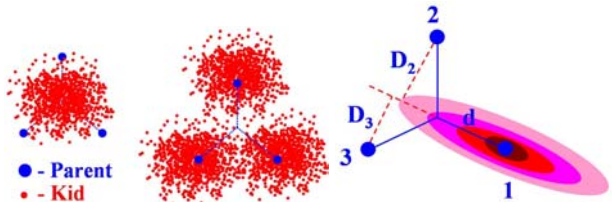

(a) (b) (c)

Figure 2: (a) UNDX operator, (b) PCX operator, (c) PCX operator: creation of the offspring

3.2.2 Algorithm for parallelizing G3 model

A multiple-population or multiple deme (or island) based GA model (Back et al., 2000; E. Cantú-Paz, 2000) was used during the analysis. To capture the effect of deme size, migration gap and number of migrated individuals, an adaptive scheme was used. In this scheme, deme size was incremented after every migration to avoid any pre-convergence. The destinations of the migrants were based on *(+1+2)* topology (E. Cantú-Paz, 2000). This topology signifies that at first epoch, machine rank *0* will receive solutions from machines ranked *1* and *2*, and will send its data to machines with rank *p-1* and *p-2*, where *p* is the total number of processors. The choice of topology also affects the quality of the search. To reduce this effect, an extended neighborhood theory and migration before convergence were used during the calculation. The extended neighborhood can be understood by imagining a tree rooted on a particular deme. The descendants of a node in the tree are the immediate neighbors of the deme it represents, and the τ-level in the tree contains the demes that are reachable from the root deme after τ epochs (E. Cantú-Paz, 2000). These demes form the extended neighborhood of the root as shown in Fig. 3. Selecting the emigrants and replacements based on their fitness may increase the selection pressure, which will influence the speed of convergence of the algorithm. Excessively slow or fast convergence rates may cause the search to fail (Goldberg et al., 1993; Thierens and Goldberg, 1993). If the selection is too weak, the population may drift aimlessly for a long time, and the quality of the solutions found is not likely to be good. On the other hand, rapid convergence is desirable, but an excessively fast convergence may cause the GA to converge prematurely to a suboptimal solution. The selection intensity is maximum when the best individuals migrate and replace

the worst. To avoid pre-convergence, the selection intensity is reduced by generating extra random individuals at each epoch.

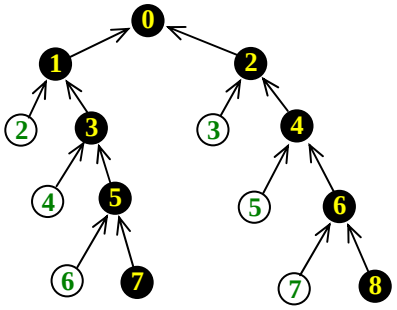

Figure 3: Tree representation of the extended neighborhoods of demes in *+1+2* topology of degree 2. The numbers inside the circle represent the processor id. (E. Cantú-Paz, 2000).

The algorithm can be summarized as follows and the flowchart is given in Fig. 4:

1. Generate different random numbers to create different population on each machine.
2. Use different values of σ_ς and σ_η on different machines to keep diversified children around the parents.
3. Assign *generation*; *epoch*; generation gap (*Gen_gap*); migrated members (*uncles*); increase in deme size (*alliens*); group members (*gp_member*);
4. Run the PCX based G3 model and keep track of best fitness value on each processor.
5. If number of generations since the last migration is greater than or equal to the generation gap (*Gen_gap*) then find the average of the best fitness values (*avg_best*) of the previous *Gen_gap* number of generations, otherwise skip to step 7.
6. If *avg_best* is equal to the best fitness for the current generation then:
   (a) Arrange the population in the order of their decreasing fitness values.
   (b) Select the partners using *(+1+2)* topology.
   (d) Exchange best solutions, equal in number to the *uncles*, with the partners.
   (e) Remove worst *uncles*2* solutions from the population.
   (e) Generate *alliens* number of new population members using different random seeds to avoid creating the same individuals.
   (f) Assign *epoch* = *epoch* + *1*;
7. Assign *generation* = *generation* + *1*; and continue till convergence.

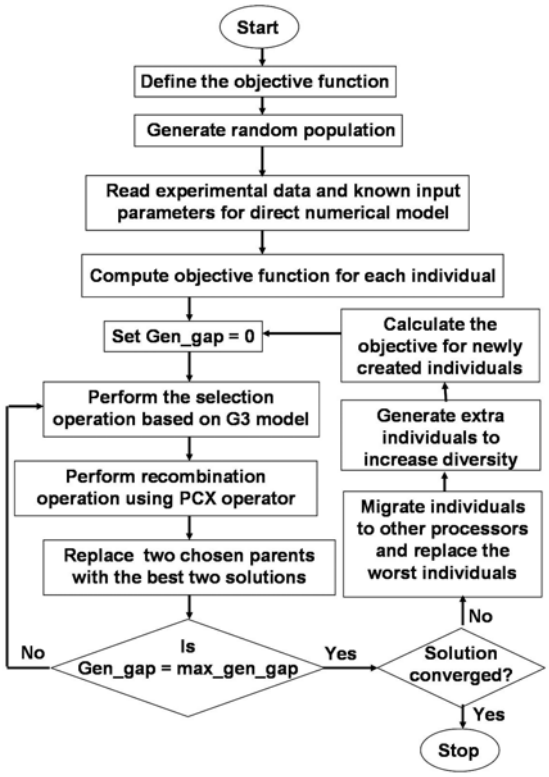

Figure 4: Flow chart of the parallelized G3 model

4 RESULTS AND DISCUSSION

In order to generate the initial random population to start the calculations, the values of the six unknown parameters were initialized based on their values reported in the literature (Elmer et al., 2003). The used initialization ranges for these variables are as follows: *P* (1.0 to 2.5 k*W*); *v* (0.3 to 1.0 *mm/s*); *k* (20.0 to 50.0 *W/m-K*); k_0 (1.0×10^5 to $2.5\times10^5 s^{-1}$); *Q* (100.0 to 150.0 *kJ/mol*); and *n* (1.0 to 2.5). All the runs were conducted using 5 different random seeds to achieve a convergence limit where 20% individuals of the total population reached an objective function value (fitness) of less than 3.0×10^{-2}.

4.1 PERFORMANCE OF THE SERIAL G3 ALGORITHM

4.1.1 Effect of computational complexity of objective function on G3 model

In order to investigate the efficacy of the G3 model with PCX operator, two different objective functions were solved. The first objective function contained only the temperature term as shown in Eq. 7.

$$\min O1 = \sum_{i=1}^{n}\sum_{j=1}^{m}\left(\frac{T^c(x_i,y_j,0)}{T^e(x_i,y_j,0)}-1\right)^2 \qquad (7)$$

The second objective function was the actual objective function described in Eq. 4, which contains both temperature and phase fraction terms. Runs were taken for 5 different random seeds with population size (N) = 100 and number of kids (λ) = 2. In order to search reliably in a large dimensional search space, smaller step sizes in variables were chosen by taking low values of σ_η and σ_ζ. Figure 5 shows that higher number of function evaluations is required for combined objective (Eq. 4). This is because first objective function (Eq. 7) is dependent only on three variables while the second objective function is a function of six variables, and increase in problem size increases the dimensionality of the search space. Figure 5 also shows that the objective function containing temperature and phase fraction terms has a number of local minima regions, where the search temporarily gets entangled. However, convergence is finally attained in each case indicating that the PCX operator based G3 algorithm is good enough to bring the solutions out of these local minima by exploring the regions outside these areas.

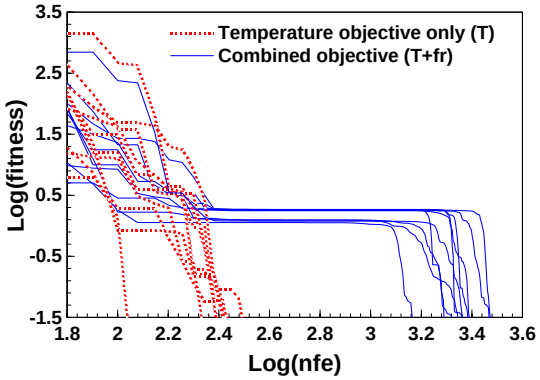

Figure 5: Variation of required number of function evaluations (*nfe*) for 10 different random seeds.

4.1.2 Effect of σ_ζ and σ_η on convergence

Different runs were taken for different values of σ_ζ and σ_η. Figure 6 shows that number of function evaluations increases with increase in σ_η and σ_ζ. Values of σ_η and σ_ζ in the range of 0.1 to 0.15 require fewer function evaluations compared to higher values of these parameters. This is because smaller values of σ_η and σ_ζ result in smaller step size in the values of variables, which facilitates good exploration near the optimal solution.

4.1.3 Effect of number of kids and parents participating in PCX on convergence

Figure 7 shows the effect of number of kids and population size on the number of function evaluations. As 20% individuals of whole population are required to reach the minimum limiting value of objective function (i.e. 3.0×10^{-2}) to terminate the calculation, more number of kids is required for exploration. Large number of kids increases the number of function evaluations. So, there exists a tradeoff between number of kids and function evaluations to attain the convergence. Figure 7 shows that number of kids in the range of 2 to 5 gives better solutions compared with large number of kids. This number is slightly higher than that suggested by (Deb et al., 2002) for Rosenbrock function analysis. This discrepancy may be attributed to the nature of objective function, which gets trapped in local minima as shown in Fig. 5. It may also be due to the strict implementation of convergence criterion on the solution. Higher number of kids helps in exploring large search space around the parents and thus, in coming out of the local traps. Increase in population does not help much in reducing the number of function evaluations because of the selection of only two best solutions from the kids and participating parents. Therefore, increase in population size only overburdens the number of function evaluations as can be seen from Fig. 7.

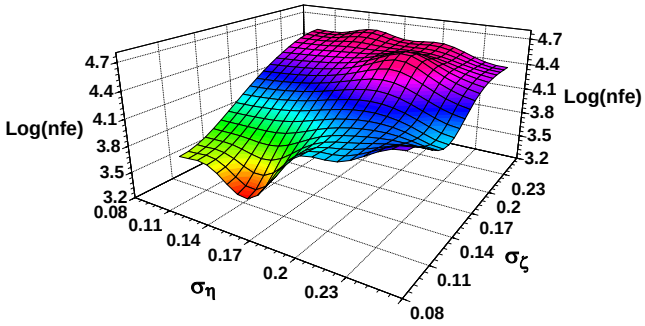

Figure 6: Variation in required number of function evaluations (*nfe*) for different values of σ_η and σ_ζ with population size (N) = 100 and number of kids (λ) = 2.

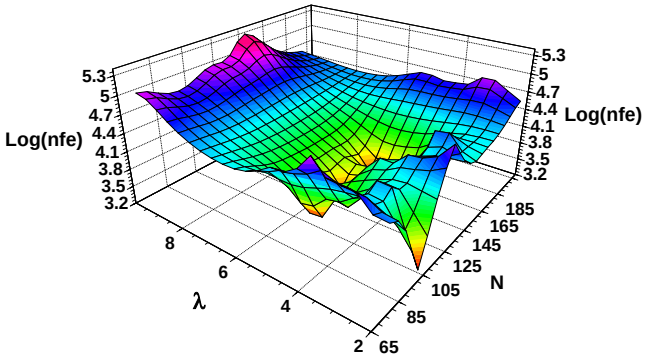

Figure 7: Variation in required number of function evaluations (*nfe*) for different values of population size (N) and number of kids (λ).

4.2 PERFORMANCE OF THE PARALLEL G3 ALGORITHM

In the parallel algorithm, different values of σ_η and σ_ζ in the range of 0.1 to 0.15 were used during the calculations because these values require lesser function evaluations as shown in Fig. 6. All the preliminary parallel computation

analysis is done on a cluster of 4 PCs of 2.86 GHz frequency and 512 MB RAM. The parallel computation time (T_P) is given by:

$$T_P = T_f + T_c = (nfe * t_f) + T_c \quad (8)$$

where T_f is the computation cost, T_c is the time spent in communication between processors and t_f is the function evaluation time. The communication time is negligible (i.e. few micro seconds) compared to function evaluation time (i.e. t_f = 3 seconds) because only the values of the variables and the corresponding objective function are transferred among processors during the communication. So, we can rewrite Eq. (8) as follows:

$$T_P \approx T_f = (nfe * t_f) \quad (9)$$

Therefore, in the present study the parallel computation time is presented in the form of number of function evaluations required for convergence. As increase in the population size does not affect the number of function evaluations required for convergence in the steady state, PCX-based serial G3 model (see Fig. 7), a deme size of 100 was used on the processors. A deme size of 100 can also help in achieving higher reliability as compared to smaller deme size, which often causes evolutionary algorithms to have low reliability (Reed and Yamaguchi, 2004).

4.2.1 Effect of the number of migrated members and migration gap (frequency)

In the migration policy, the best migrants replace the worst individuals, which is a case of high selection pressure. At each epoch, extra random individuals are also generated to reduce the selection pressure and increase the diversity. If the migration frequency is too high (i.e. generation gap between migrations is low), then the selection pressure increases due to faster diffusion of best solutions among processors. This may lead to pre-convergence or localized exploration of the solution space. If the migration frequency is too low (i.e. generation gap between migrations is high), then diffusion of best solutions will require more generations to reach the other processors, resulting in relatively more number of function evaluations, as is evident from Fig. 8. This may be due to wastage of time in exploring the local region. Increase in migrated members also increases the selection pressure. At low value of migration gap and large number of migrated members, selection pressure is highest. Therefore, the algorithm requires more function evaluations to avoid pre-convergence, as shown in Fig. 8.

4.2.2 Effect of number of migrant individuals and randomly created extra individuals (*alliens* or increment in deme size) at each epoch

In the migration policy, if there is no increment in deme size, and if large number of migrated best members replace the worst solution, then the selection pressure is high. This may lead to pre-convergence of solution. Increase in deme size at each epoch reduces this selection pressure, and hence the algorithm requires less function evaluations to reach the convergence limit as shown in Fig. 9. Too much increase in deme size puts extra burden of objective function evaluation for newly created individuals. Therefore, a small optimal value should be chosen to increase the diversity and avoid any pre-convergence.

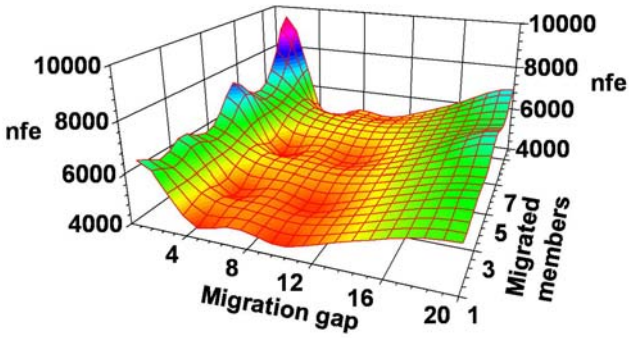

Figure 8: Variation in required number of function evaluations (*nfe*) for different values of migration gap (or frequency) and migrated members (or migration rate).

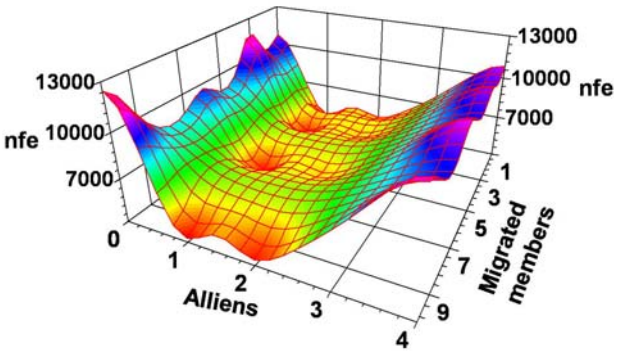

Figure 9: Variation in required number of function evaluations (*nfe*) for different number of migrated members (i.e. migration rate) and number of randomly created individuals at each epoch (i.e. *alliens*).

4.2.3 Speedup and reliability

The speedup is defined as:

$$S_p = \frac{T_s}{T_p} \approx \frac{(nfe)_s \times t_f}{(nfe)_p \times t_f} = \frac{(nfe)_s}{(nfe)_p} \quad (10)$$

where T_s is the time required on single processor while T_p is the time required on p-processors to achieve the same convergence limit. Equation (10) shows that if the communication time is negligible compared to function evaluation time, then the speed up is equal to the ratio of number of function evaluations (*nfe*) required on single processor to *nfe* on p-processors for same convergence.

Figure 10 presents the effect of the number of processors on number of function evaluations required, *nfe*, for achieving the desired convergence criteria. Each box-plot

summarizes the result for 25 random runs. Different random seeds and different parameter values (e.g. σ_η and σ_ζ) were used on different processors. Figure 11 summarizes the success/failure (in percentage) of achieving the convergence within 50,000 number of function evaluations. Only the data for the successful runs are plotted in Fig. 10. The outer intervals or the lines of the box plots in Fig. 10 represent the number of function evaluations (*nfe*) for 95th percentile confidence interval (CI), while the notches (or boxes) represent the 75th percentile CI, and the horizontal line inside the notch (or box) designates the median. The standard deviation in the number of function evaluations on a single processor is very large, as can be seen in Fig. 10. However, the standard deviation decreases drastically for more than four processors. Figure 10 shows that almost linear speed-up was attained for smaller number of processors. With increase in the number of processors above four, the standard deviation in the number of function evaluations decreased drastically. Figure 11 shows that the reliability of the model increases significantly with increase in the number of processors. This framework with more than four processors produces a success rate of close to 95% for solving the proposed problem. The above increase in speedup and reliability for higher number of processors may be due to the effect of using different parameter values on different processors, migration rate, migration frequency and the number of extra individuals created at each epoch, because these help in exploring the diverse region simultaneously and in avoiding the local minima. The faster convergence is the key advantage of the PCX based G3 model (Deb et al., 2002; Deb, 2003) over other existing evolutionary algorithms. By increasing the reliability using multiple processors, this framework will be very helpful in solving the real-world problems where reliability and faster convergence are the two main requirements.

4.3 VALIDATION OF THE OBTAINED VALUES OF UNKNOWN PARAMETERS

An important advantage of genetic algorithm optimization technique is that it provides the practicing engineer with a window of input variables that would lead to a target weld geometry and microstructure. Table 3 clearly illustrates this advantage where six different sets of input parameter values obtained from the smart model have been listed, all of which can give the required weld geometry and microstructure. The calculated values are within the acceptable limits as reported in the literature; for example, (Christian, 2002) suggested that the value of the JMA exponent, *n*, should lie between 1.5 and 2.5 for diffusion controlled transformations, and (Elmer et al., 2003) determined *n* to be 1.45; also, (Elmer et al., 2003) used a value of *Q* equal to 117 kJ/mole.

In situ Spatially Resolved X-Ray Diffraction (SRXRD) experiments provide direct observation of welding induced phase transformations (Elmer et al., 2003). Figure 12 shows an experimentally measured phase map in the heat-affected zone (HAZ) on the top surface of gas tungsten arc (GTA) weld in AISI 1005 C-Mn steel (Elmer et al., 2003). This phase map gives quantitative information about the changes occurring in the austenite (γ) volume fraction during the heating cycle. The shading indicates the fraction of austenite, which varies from 0% austenite (γ) (blue portions or dark shade starting at y = 9 mm location) to 100% austenite (red portions or dark shade close to the center of the figure). The thick solid lines in Fig. 12 represent temperature isotherms calculated by the Rosenthal equation (Eq. 1) using the input parameters predicted by the current smart model, i.e. the first set of values in Table 3. The weld pool boundary is marked by the solidus isotherm (1779 K), while the *A1* (993 K) and *A3* (1204 K) isotherms identify the equilibrium start and finish locations for the ferrite to austenite ($\alpha \rightarrow \gamma$) transformation. The calculated isotherms are found to very well mark the weld pool boundary and the austenite start and finish boundaries shown in the measured data. Thus the reliability of the parameters obtained from the smart model is ascertained.

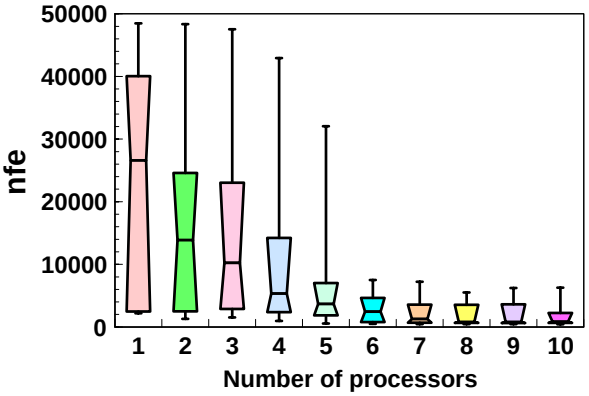

Figure 10: Variation in required number of function evaluations (*nfe*) with number of processors.

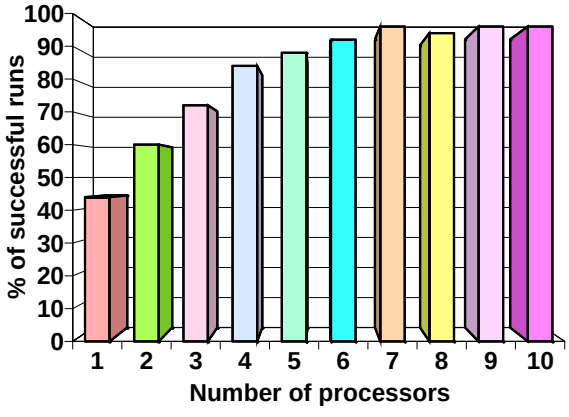

Figure 11: Percentage of successful (converged) runs for different number of processors.

The internal consistency of the kinetic parameters obtained from the smart model, reported in Table 3, was checked by comparing the austenite fractions at different SRXRD locations, presented in Table 1, with those calculated by the non-isothermal JMA equation (Eq. 2) using the first set of values in Table 3. The calculated austenite fraction curve in Fig. 13 almost overlaps the experimental data showing the accuracy of the kinetic parameters obtained by the smart model. Fig. 13 also shows that the calculated curve is in much better agreement than that reported in the literature (Elmer et al., 2003), which was obtained using conventional data fitting approach.

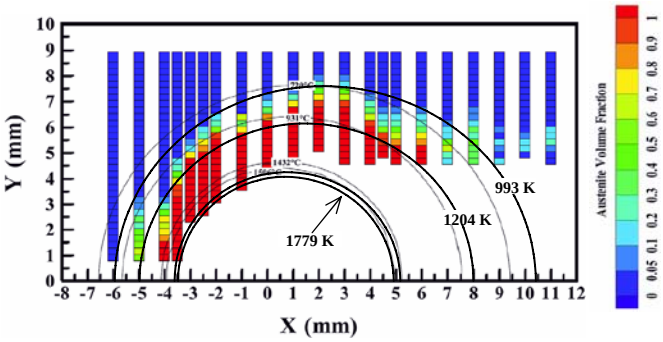

Figure 12: The top surface of the weld with experimentally measured austenite phase fractions. The thin, grey, solid lines are the temperature isotherms calculated by (Elmer et al., 2003). The superimposed thick solid lines represent the temperature isotherms calculated in the present study by using the optimized values of unknown parameters in the Rosenthal equation.

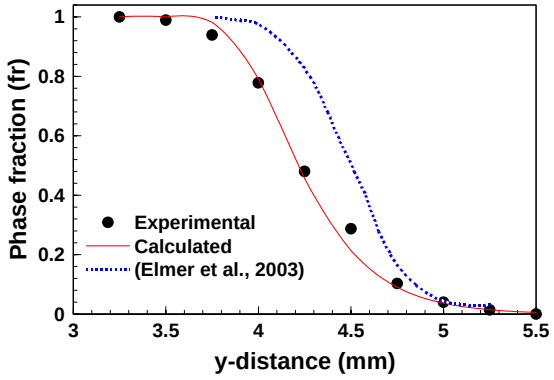

Figure 13: Comparison of the calculated and experimentally obtained transformed fractions of γ-austenite at a given x-location (x = -3.5 mm) in the weld heat-affected zone. The results are compared with those calculated by (Elmer et al., 2003) for the same location.

It is noteworthy, that the smart model used the experimental data for only one x-location in the HAZ (x = -3.5 mm, given in Table 1) to calculate the unknown input parameters. To analyze if these parameters can be used to predict the γ-fractions at other x-locations in the HAZ, the calculated results for two other x-locations (x = 0 mm and 1 mm) were compared with the corresponding experimental measurements in Fig. 14. The calculations were done using the last set of unknown parameter values given in Table 3. Fair agreement is seen in all the cases indicating the robustness of the smart model in predicting the microstructure in the HAZ, while using only a limited set of input experimental data.

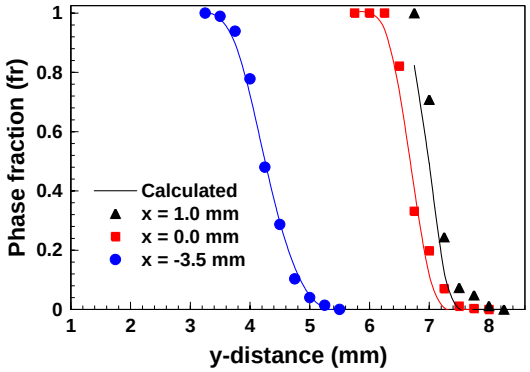

Figure 14: Comparison of the calculated (lines) and the experimentally obtained (symbols) transformed γ-fractions at different x-locations in the HAZ.

Table 3: Different sets of unknown parameters obtained from the smart model.

P (kW)	v (mm/s)	k (W/m-K)	Q (kJ/mol)	n	k_0 (s^{-1})
1.68	0.59	37.49	116.56	1.43	1.84×10^5
1.59	0.56	35.29	112.31	1.77	1.47×10^5
1.75	0.62	38.99	114.59	1.49	1.46×10^5
1.71	0.60	38.10	113.57	1.66	1.30×10^5
1.82	0.64	40.70	112.66	1.90	1.49×10^5
1.72	0.61	38.33	114.83	1.43	1.70×10^5

5 CONCLUSIONS

A smart phenomenological model for GTA butt welding involving parallel genetic algorithm and phenomenological models of temperature field and phase fraction calculation was developed. The smart model was used to estimate the net input power, effective thermal conductivity, welding speed, activation energy of transformation, pre-exponential and exponent of Johnson-Mehl-Avrami (JMA) equation from a limited set of experimental data. The following conclusions can be drawn from the study.

(1) The Parent Centric Recombination (PCX) based Generalized Generation Gap (G3) model is able to explore the search area even in large search dimensions without getting trapped in local minima. The convergence of the model is not very sensitive to the population size.

(2) Too high or too low migration frequency degrades the performance of the parallel model because of the increased selection pressure and low diffusion rate of best solutions, respectively.

(3) A small optimal value of deme size increment gives best performance as it allows an increase in diversity while avoiding any pre-convergence due to high selection pressure used in the algorithm.

(4) The reliability of the PCX based G3 model increases drastically with increase in the number of processors. The proposed framework is highly efficient for solving real world problems due to its faster convergence and higher reliability on multiple processors.

(5) Different sets of values of the unknown parameters, i.e. net input power, effective thermal conductivity, welding speed, activation energy of transformation, pre-exponential and exponent of Johnson-Mehl-Avrami (JMA) equation, were estimated by the model using only a limited amount of experimental data. When these estimated unknown parameter were used as inputs in the phenomenological models to calculate the γ-fractions in the HAZ, the results agreed very well with the corresponding experimental measurements indicating the accuracy of the predictions. The agreement of these results was much better than that of the results reported in the literature.

Furthermore, the application and the effect of various parameters on convergence of parallel island based PCX-G3 model described in this paper is a contribution to the growing knowledge base in the field of evolutionary algorithms.

Acknowledgments

The authors would like to express their gratitude to Mr. W. Zhang for assisting with the phase transformation calculation model. The authors are also thankful to Dr. K. Deb and KANGAL lab members for providing free access to their PCX operator based G3 model.

References

T. Back, D. B. Fogel, and Z. Michalewicz (eds.) (2000). *Handbook of Evolutionary Computation*s. IOP Publishing Ltd.: Oxford University Press.

E. Cantú-Paz (2000). *Efficient and Parallel Genetic Algorithms*. Boston:Kluwer Academic Publishers.

J. W. Christian (2002). *The Theory of Transformations in Metals and Alloys, 3rd edition*. Boston:Pergamon.

S. A. David and T. DebRoy (1992). Current issues and problems in welding science. *Science* **257**:497-502.

A. De and T. DebRoy (2004). A smart phenomenological model for probing unknown welding parameters. *Journal of Physics D: Applied Physics* **37**:140-150.

K. Deb, A. Anand, and D. Joshi (2002). A computationally efficient evolutionary algorithm for real-parameter optimization. *KanGAL Report No. 2002003, April*.

K. Deb (2003). A population-based algorithm-generator for real-parameter optimization. *KanGAL Report No. 2003003, March*.

J. W. Elmer, T. A. Palmer, W. Zhang, B. Wood, and T. DebRoy (2003). Kinetic modeling of phase transformations occurring in the HAZ of C-Mn steel welds based on direct observations. *Acta Materialia* **51**:3333-3349.

D. E. Goldberg, K. Deb, and D. Thierens (1993). Toward a better understanding of mixing in genetic algorithm. *Journal of the Society of Instrument and Control Engineers* **32**(1):10-16.

V. A. Karkhin, V. V. Plochikhine, and H. W. Bergmann (2002). Solution of inverse heat conduction problem for determining heat input, weld shape, and grain structure during laser welding. *Science and Technology of Welding and Joining* **7**:224-231.

A. Kumar, W. Zhang, C.-H. Kim, and T. DebRoy (2004). A smart bi-directional model of heat transfer and free surface flow in GMAW for practicing engineers. In *7th International Seminar on Numerical Analysis of Weldability at Graz, Austria*. (In press)

A. Kumar and T. DebRoy (2004). Guaranteed fillet weld geometry from heat transfer model and multivariable optimization. *International Journal of Heat and Mass Transfer*. (Submitted for publication)

S. G. Lambrakos and J.O. Milewski (2002). Analysis of processes involving heat deposition using constrained optimization. *Science and Technology of Welding and Joining* **7**:137-148.

S. K. Nath, S. Ray, and V. N. S. Mathur (1994). Non-isothermal austenisation kinetics and theoretical determination of intercritical annealing time for dual-phase steels. *The Iron and Steel Institute of Japan* **34**:191-197.

P. Reed and S. Yamaguchi (2004). Simplifying the parameterization of real-coded evolutionary algorithms. *2004 EWRI World Water and Environmental Resources Congress*. Salt Lake City. (In press)

S. Sista, Z. Yang, and T. DebRoy (2000). Three-dimensional Monte Carlo simulation of grain growth in the heat-affected zone of a 2.25Cr-1Mo steel weld. *Metallurgical and Materials Transactions B* **31**:529-536.

D. Thierens and D. E. Goldberg (1993). Mixing in genetic algorithms. In S. Forrest (ed.), *Proceedings of the Fifth International Conference on Genetic Algorithms*, 38-45. San Mateo, CA: Morgan Kaufmann.